 Svenox	Project number 90 019 000	Document number 90 019 017
	Issue 001	Design Phase N/A
Customer Internal project		Date 2009-06-29
Project name Drnr. AL90 A 2008 70787	Document type Final Report	Classification

Slutrapport för EMFO-projektet: "Avancerade partikelefterbehandlingssystem för tunga dieselmotorer, EU6 och framåt"

Sammanfattning

Kommande lagkrav med avseende på emissioner i såväl Europa (EU6) som USA (US10) kommer troligen kräva kombinerade efterbehandlingssystem. Här betyder det en kombination av partikelfällor och SCR system. Var för sig har dessa system funnits på marknaden men nya utmaningar uppstår när de två skall sammanföras till en enhet som dessutom i stark grad är kopplad till motorstyrningen. Syftet med projektet var att öka kunskapsnivån i företaget inom filterområdet med focus på kombinerade system och har involverat modellering, komponentutprovning samt olika studier av aktiv regenerering och effekterna av detta på kringliggande komponenter.

Projektet har varit mycket lyckosamt både vad gäller att höja företagets allmänna kompetensnivå samt att bygga upp ett samarbete med högskola inom sotoxideringsområdet. Dessutom har projektet även resulterat i ett simuleringsverktyg för filter och ett antal vetenskapliga publikationer.

Summary

The forthcoming emission legislations in Europe (EU6) as well as USA (US10) will most likely require combined aftertreatment systems, which in this case means a combination of particulate filters and SCR system. Separately, these systems have been commercially available. However, new challenges arise when the two are implemented in the same unit, which additionally is highly coupled to the engine management. The aim of the project was to increase the company knowledge within the filter area focusing on the combined systems and it included modelling, component testing and different studies on active regeneration and the effect on surrounding parts.

The project has been very successful, both regarding the general increase of the competence level within the company and to build a collaboration with university within the soot oxidation area. Further has the project resulted in a number of useful tools and methods have been developed. In addition, the project has also resulted in a number of scientific publications.

Written by:
Mikaela Wallin

Svenox AB
Commercial Vehicle Exhaust Systems

Technical Centre
Victor Hasselblads gata 6
SE-421 31 V:a Frölunda
Sweden

<http://www.svenox.com>

Tel: +46 (0)31 724 79 00
Fax: +46 (0)31 724 79 99
E-mail: engineering@svenox.com

Contents

Sammanfattning	1
Summary	1
1 Introduction.....	3
2 Modelling	3
2.1 Soot storage and oxidation model	3
2.1.1 Symbols	3
2.1.2 Abbreviations	3
2.1.3 Prerequisites	4
2.1.4 Modelling.....	4
2.1.5 Gas transport	4
2.1.6 Soot particle filtration	5
2.1.7 Soot particle oxidation kinetics.....	6
2.1.8 Parameter fitting to experimental data	7
2.1.9 Input data to the structure	7
2.1.10 Pre-processing a simulation.....	7
2.1.11 Start a simulation	8
2.2 SCR model	14
2.2.1 Modelling.....	14
2.2.2 Parameterisation for Fe-zeolite SCR catalyst	15
2.2.3 Experimental data.....	15
2.2.4 Model setup	16
2.2.5 Iron sites	17
2.2.6 Zeolite-sites	19
2.2.7 Parameterization.....	21
2.2.8 Results.....	23
2.2.9 Discussion.....	27
2.2.10 Conclusion	29
2.2.11 Symbols	29
2.2.12 Symbol units	30
2.2.13 Chemical species.....	31
3 Bibliography	31

1 Introduction

The forthcoming emission legislations in Europe (EU6) as well as USA (US10) will most likely require combined aftertreatment systems, which in this case means a combination of particulate filters and SCR system. Separately, these systems have been commercially available. However, new challenges arise when the two are implemented in the same unit, which additionally is highly coupled to the engine management. The project focus is on the particulate filter part of these combined systems and will involve modelling, construction and validation of demonstrators and testing of components. This report focus on the theoretical part of the work such as soot modelling and updating the SCR model.

2 Modelling

2.1 Soot storage and oxidation model

A model structure for simulating a Diesel particle filter has been generated. It is capable of obtain a pseudo 3D solution of the characteristics of the DPF. The model structure contains physics for the filtration of the soot particles, oxidation of the soot and the equilibrium between the two NO_x components. It is possible to use the geometries of the 2D surfaces used in the CZM-software at Swenox.

Previous work at Swenox [1,2] has been focused on the SCR-catalyst. With the stricter legislations with respect to particle emissions from the diesel engines a model structure that simulates the physical and chemical processes in the filter is desirable. By using simulations for predicting the filter behaviour at varying loads an improved product development may be achieved.

2.1.1 Symbols

α = specific filtration resistance, [m/kg]
 c = weight of dry cake / filtrate volume, [kg/m³]
 c_i = Concentration of component i [mol/m³]
 E_a = Reaction activation energy [J/mol]
 $K_{1,2,3,4,5 \text{ or } 9}$ = Kintetic rate constant [variable]
 R = Universal gas constant
 R_c = resistance of cake, [m⁻¹]
 R_m = resistance of filter medium, [m⁻¹]
 T = Temperature [K]
 u = Filtrate flow [m/s]
 w = weight of dry cake / area, [kg/m²]
 y_i = Mole fraction of component I [-]
 μ = Viscosity of fluid [m²/s]

2.1.2 Abbreviations

CFD	Computational fluid dynamics
DPF	Diesel particle filter
SCR	Selective catalytic reduction

2.1.3 Prerequisites

The developed model structure should be compatible with the model that has been developed for the SCR-Catalyst [1,2] in terms of the following:

- The output from the model structure has to be compatible with the input to the SCR-model.
- The geometrical shapes, i.e. circle, double, race track and etc, that are used in the SCR-model should be used in the model structure.
- It should be possible to use the input data from CFD that is used in the SCR-model.

The model structure should contain the core physics of the DPF, i.e. filtration physics and soot oxidation kinetics.

2.1.4 Modelling

The developed model is based on the flow in one inlet and outlet channel of the diesel particle filter. This pair of channels is assumed to have no connection with the other channel pairs. The filter length is divided into a number of elements as shown in Figure 1. The number of divisions may be altered by the user.

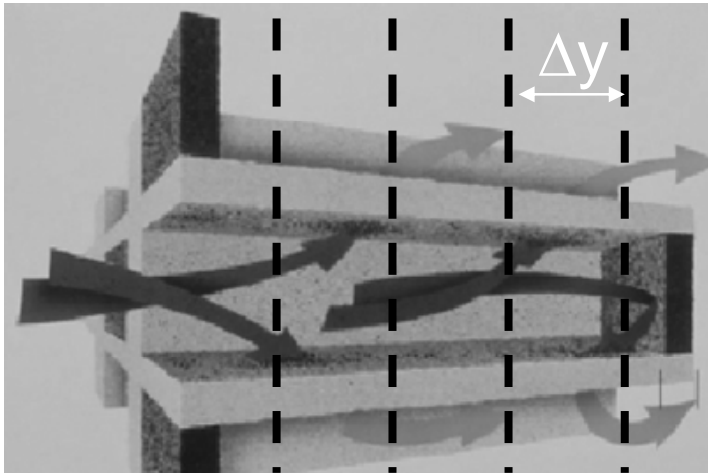


Figure 1: Schematic image of the division of the DPF into an arbitrary number of cells along the filter length.

In each the gas and particle transport is solved together with the filtration and oxidation of the soot particles. These models will briefly be described in the subsequent sections. The heat transfer between different inlet channels and the heat capacity of the DPF-material has been neglected. Plug flow in the channels and no spatial variation (except in the length of the filter) in composition and temperature is assumed.

The 2D-surface for translating CFD data to input data for the existing SCR-module is used in the DPF model structure. Thus a pseudo 3D-solution for the particle filter is obtained. Physical data for the gas components (CO , CO_2 , N_2 , NO_2 , NO , O_2) is obtained from [4].

2.1.5 Gas transport

Figure 2 show one calculation cell with the main flow paths illustrated. The transport equation [3] for each species is solved within each of these cells.

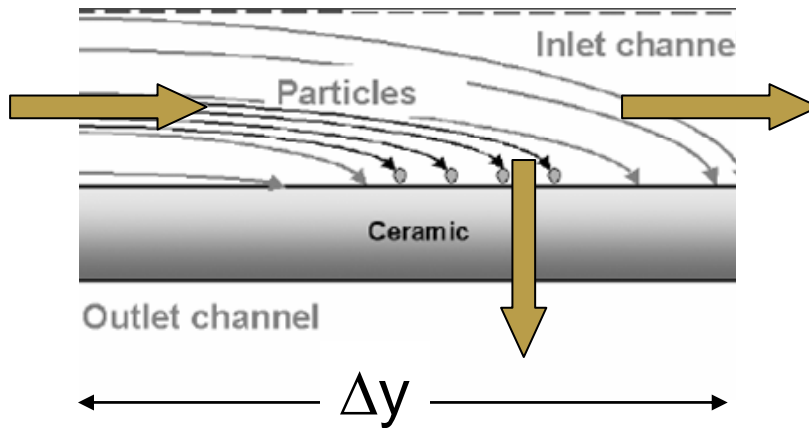


Figure 2: Schematic illustration of the gas transport in one of the calculation cells. The arrows indicate the gas flow.

The soot is treated as two different species, one for the soot present in the gas phase and one for the soot present in the filter cake. The amount of soot in each phase is governed by the source term described by the filtration equation.

2.1.6 Soot particle filtration

Figure 3 shows the individual contributions to the total pressure drop over the filter. The contribution from the channel remains almost unaffected throughout the process. Thus this physical effect may be excluded from the developed model. The same applies for the pressure contribution from the ceramic support, although the pressure increase is slightly higher. This increase is due to the migration of smaller soot particles into the support prior to the filter cake development.

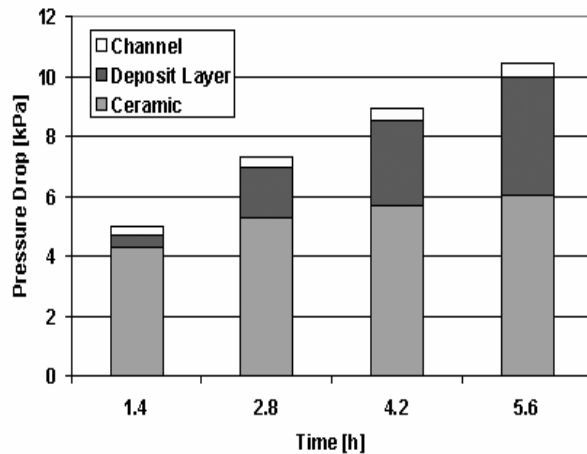


Figure 3: The individual contributions on the total pressure drop over a DPF [5]

Thus, in the developed model, the only process that causes the pressure to increase is the filter cake. It is assumed in the present model that the filter is perfect, i.e. no soot particles is emitted from the filter. Figure 4 shows a principal sketch of the filter cake with the cross flow of exhaust gases and the filtrate flow through the filter cake and ceramic.

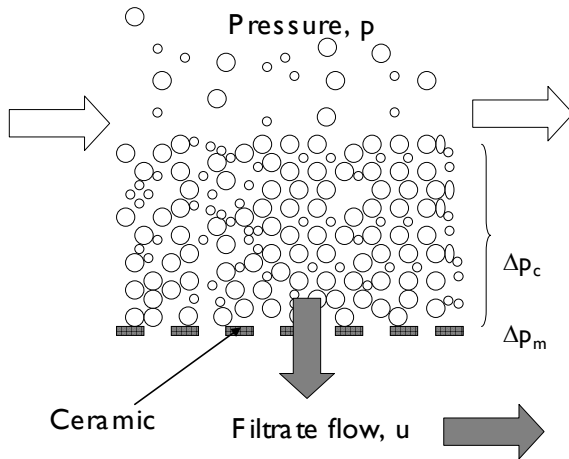


Figure 4: Principal sketch over the soot filter cake.

The filtrate flow u may be expressed as follows

$$u = \frac{1}{A} \frac{dV}{dt}$$

$$u = \frac{p}{\mu} \left(\frac{1}{R_c + R_m} \right)$$

$$\alpha = \frac{R_c}{w}$$

$$c = \frac{wA}{V}$$

$$\Rightarrow \frac{dV}{dt} = \frac{A^2 p}{\mu(\alpha c V + A R_m)}$$

Where:

u = Filtrate flow m/s

μ = Viscosity of fluid m²/s

R_c = resistance of cake, m⁻¹

R_m = resistance of filter medium, m⁻¹

α = specific filtration resistance, m/kg

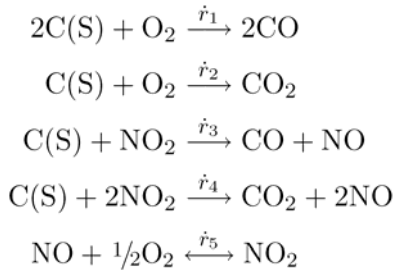
w = weight of dry cake / area, kg/m²

c = weight of dry cake / filtrate volume, kg/m³

The filtration equation is added to the transport equations as a source term for each species, including the soot as mentioned previously.

2.1.7 Soot particle oxidation kinetics

In the present model the soot is reacting with the gas species only if it is present in the filter cake. The modelled kinetics for the soot oxidation and the reaction of NO_x with oxygen may be described with the following simple reactions [6]:



Where each reaction rate may be described with the following kinetics [6] each in [kmol/(m³s)]:

$$\dot{r}_1 = f_{\text{CO}} \cdot K_1 \cdot e^{\left(\frac{-E_{a,1}}{R \cdot T_s}\right)} \cdot y_{\text{O}_2}$$

$$\dot{r}_2 = (1 - f_{\text{CO}}) \cdot K_1 \cdot e^{\left(\frac{-E_{a,1}}{R \cdot T_s}\right)} \cdot y_{\text{O}_2}$$

$$\dot{r}_3 = K_3 \cdot e^{\left(\frac{-E_{a,3}}{R \cdot T_s}\right)} \cdot y_{\text{NO}_2}$$

$$\dot{r}_4 = K_4 \cdot e^{\left(\frac{-E_{a,4}}{R \cdot T_s}\right)} \cdot y_{\text{NO}_2}$$

$$\dot{r}_{5,9} = K_{5,9} \cdot e^{\left(\frac{-E_{a,5,9}}{R \cdot T_s}\right)} \cdot \left(c_{\text{NO}} \cdot c_{\text{O}_2}^{0.5} - \frac{c_{\text{NO}_2}}{K_{\text{Equ}}(T_s)}\right)$$

$$f_{\text{CO}} = \left[1 + 0.2 \cdot y_{\text{O}_2}^{0.21} \cdot e^{\left(\frac{3000}{R \cdot T_s}\right)}\right]^{-1}$$

This kinetics can be replaced by a more detailed chemistry currently developed by Chalmers (KCK). Special care has been taken when preparing the model structure in order to obtain a simple interface for altering the kinetics. The temperature effects due to the reactions have been included in the structure by enthalpy calculations and an energy balance over each cell in the filter.

2.1.8 Parameter fitting to experimental data

The parameters in the model structure were fitted to experimental exhaust data for a existing DPF at Svenox using a least square method.

2.1.9 Input data to the structure

The input data to the model structure is obtained by running the SCR model.

2.1.10 Pre-processing a simulation

The main Matlab file for the DPF code is “DPF_main.m”. This file calls other Matlab files that take part in the computations. The user needs to set the inlet gas composition using the file “exhaustGasComposition.m”, using the following parameters:

- RohSoot: the density of the soot [kg/s].
- M_EG: total mass flow rate of exhaust gases [kg/s].
- ViscAir: viscosity of the exhaust gases [m²/s].
- Molar fractions of O₂, CO₂ and CO [-]
- Mass fraction of soot [-]
- Initial load of soot in the filter [kg]

The physical dimensions of the filter such as length, number of cells and frontal area should be set in “DPF_main.m”. During the transient simulation, the temporal evolutions

of some of the variables are monitoring in forms of figures. The user can decide the frequency (each time step or more) for displaying these figures on the screen by setting the variable “DrawEveryTimeStep”. It should be noted though that the more often the results are updated in the figure the slower the simulation proceeds. The user may turn off these figures by setting two flags (set variables equal to 0) for the lumped and distributed solution respectively. The flags are given below:

- Draw_lumped_transient, for the lumped solution
- Draw_distribution_transient, for the distribution, observe very long simulation times if set to 1

An additional flag may be used to only run the lumped solution by setting the variable Run_distribution to 0 in order to skip the distribution calculations

2.1.11 Start a simulation

The user starts the simulation by running the Matlab file “DPF_main.m”. This file starts the core of the code which is located in the Matlab file, “DPF.m”. The inputs to this file are a vector and a matrix. The vector consists of two values as follow:

- The frontal area of the filter [m²] and
- The length of the filter [m].

The matrix consists of the following vectors:

- Time [s]
- Inlet mass flow rate [kg/s]
- Inlet temperature [K]
- Inlet pressure [pa]
- Inlet molar flow of NO [mol/s]
- Inlet molar flow of NO₂ [mol/s]

The first part of the code calculates a lumped solution of the filter by considering the entire filter as one channel. Figure 5 shows the spatial distribution of the different components mole fraction during the run.

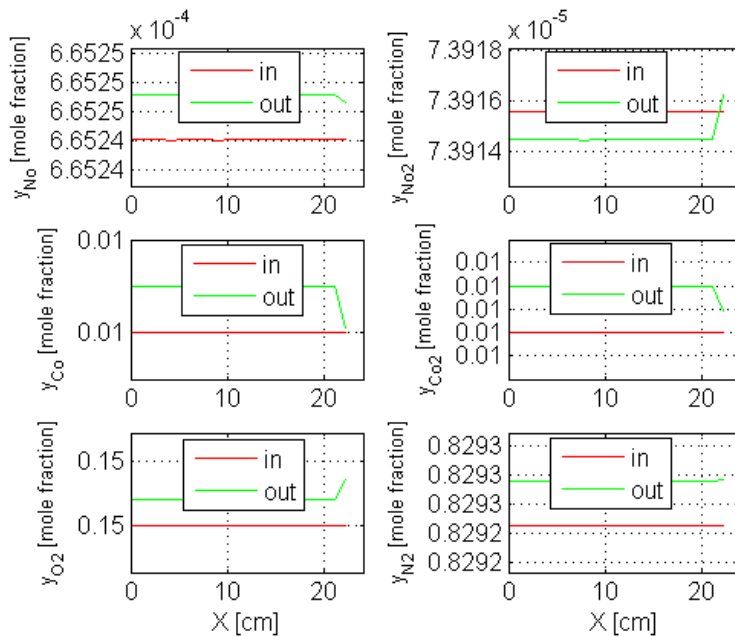


Figure 5. Spatial distribution of the mole fraction of the different components.

Figure 6 shows the temporal distribution of the pressure drop through the filter with time together with the spatial distribution of the average height of the soot layer in the filter during the time. To see the evolution of these parameters the user should use a very small time step with a very short time of about 0.1 s.

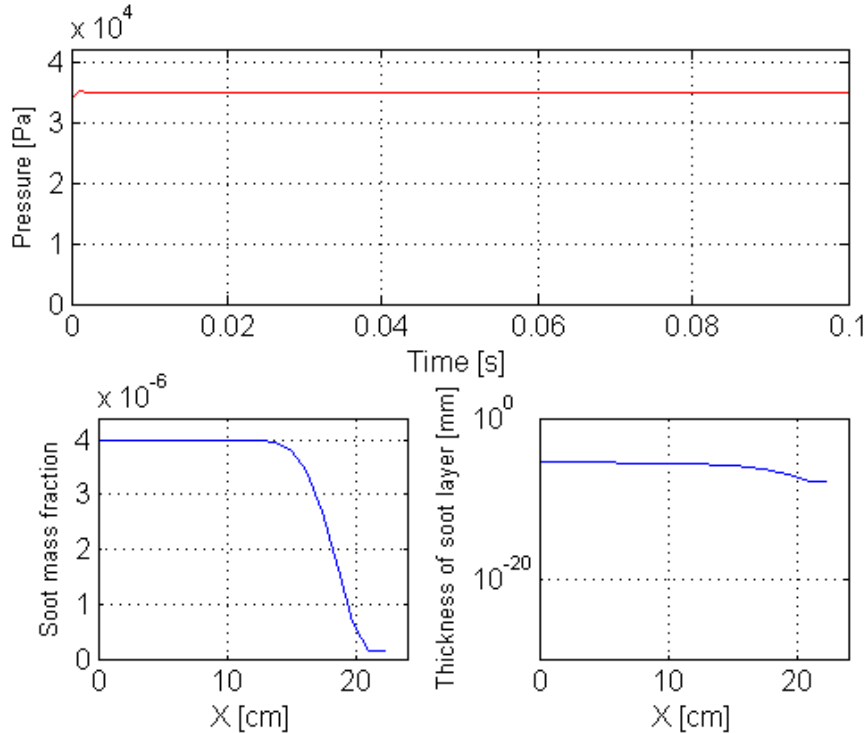


Figure 6. Evolution of the pressure drop through the filter and thickness of the soot layer.

The output of the transient simulation is two matrices; “inlet_data” and “output_data”.

The matrix “inlet_data” contains all the information about the inlet conditions to the filter while the matrix “output_data” contains all the information regarding the output gasses from the filter at each time step.

In order to draw the output from the filter with time and see the difference between the input component and the output ones the user can set the variable “output_data” to 1. In this case the code will draw figures similar to those given in figures 7-11.

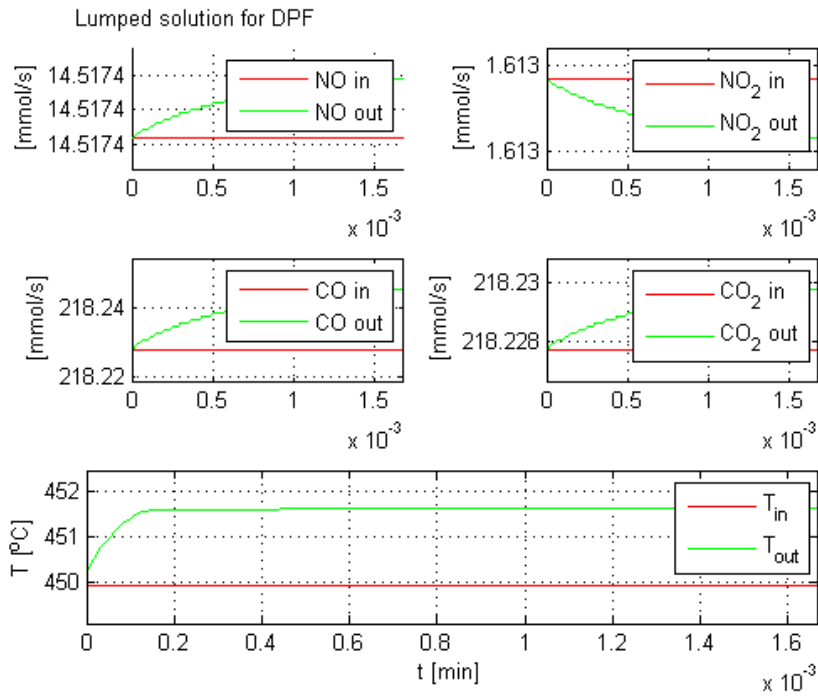


Figure 7. Output molar flow and temperature.

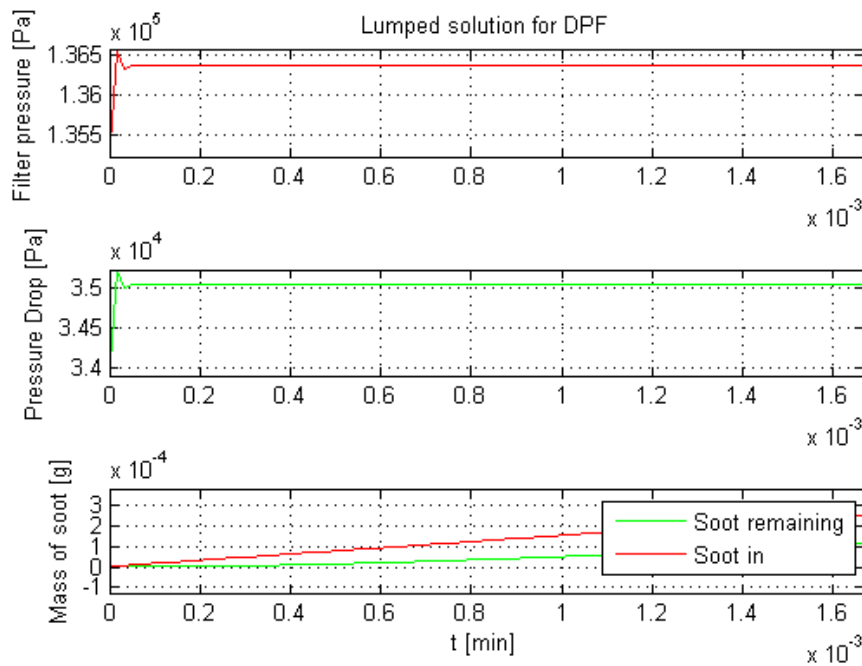


Figure 8. Output pressure drop and mass of soot.

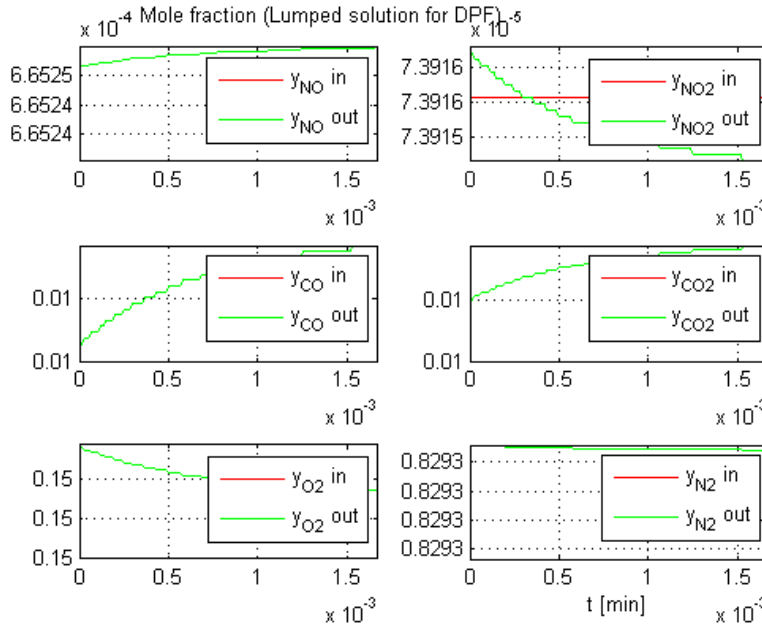


Figure 9. Output molar fraction of the components.

The remaining part of the DPF-code recalculates the diesel particle as in the case of the lumped solution with the difference that each cell in the cell and zones model is simulated. Thus a pseudo 3D-solution of the diesel particle filter may be obtained. The code draw compare the results from the entire filter as one channel and the output from the 2D filter and draw the comparison in a form of figure as shown in figure 10.

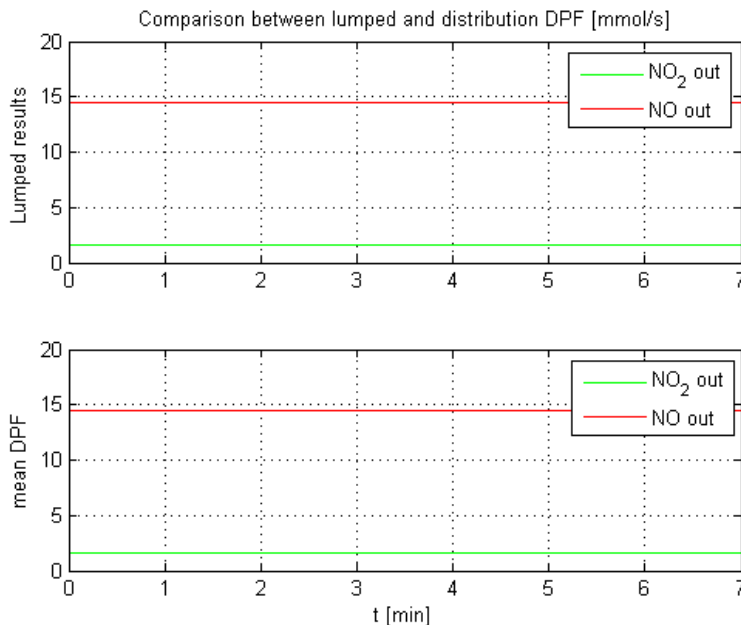


Figure 10. Comparison between lumped solution and the 2D solution.

After the simulation the 2D distributions of the different components are shown in three different times. These three different times the user can specify them in the vector “p_plots”. Typical results from the 2D model are shown in figures 11 and 12.

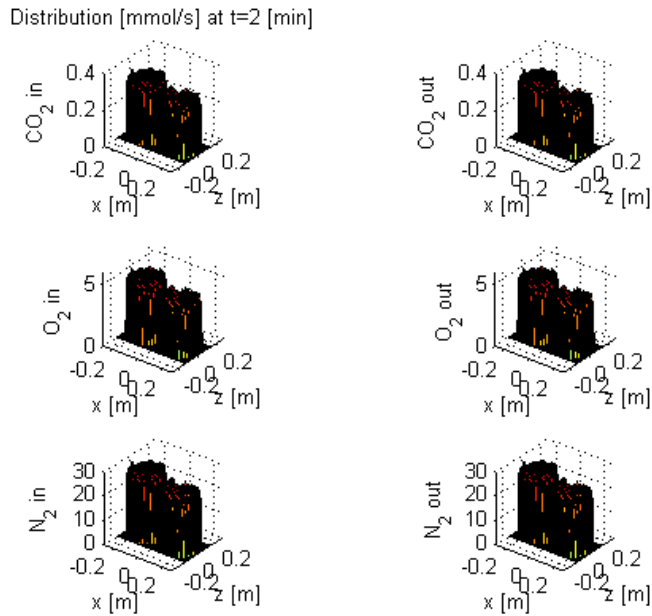


Figure 11. 2D distribution of different components mole flow rate at inlet and outlet of the filter after 2 minute from start.

T, P and Soot at t=3 [min]

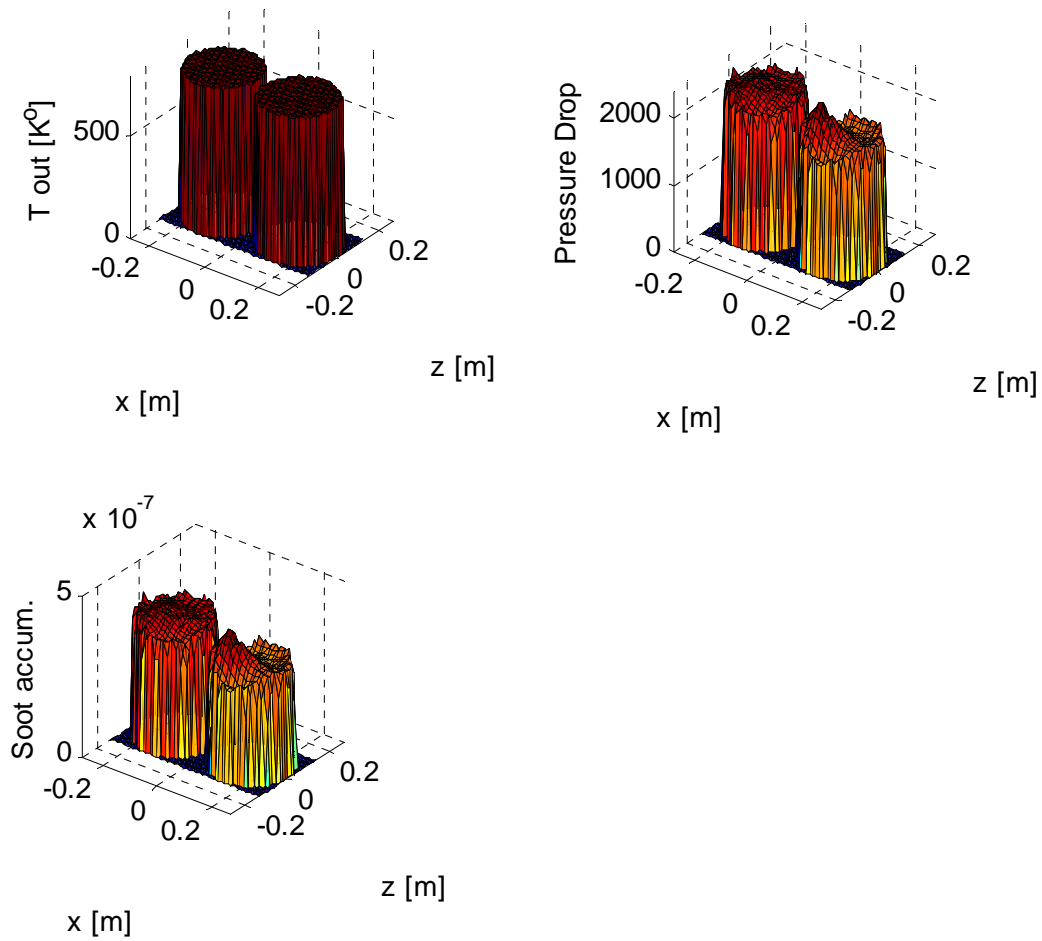


Figure 12. Outlet distribution of pressure drop temperature and soot accumulation in the filter with the double geometry.

2.2 SCR model

Swenox have previously developed an SCR model based on the SCR mechanism of the vanadia-based SCR catalyst. In the case of active regenerated filters, the temperature exceeds the limit of what these catalyst can withstand long term and the use of the more temperature stable alternative Fe-zeolite catalyst have become more common. Hence to be able to use the Swenox SCR model in most cases of combined aftertreatment systems with active regenerated filters there is a need to adjust the model to the Fe-zeolite catalysts with a more suitable chemical mechanism and to fit the parameters to experiment using Fe-zeolite catalysts.

2.2.1 Modelling

Chemical reactions are usually expressed mathematically in the form of reaction rates (r), an example of reaction rate expression is given by Equation 1. The reaction rate constants (k) are usually expressed by the Arrhenius equation (Equation 2). For the reactions above in some cases the species involved could be either on the surface or in the gas phase. For specie j on the surface the amount is expressed as the surface coverage Θ_j . For a gas phase specie i the amount is expressed in terms of concentration c_i . A_x is the pre-exponential factor for a reaction x , E_a is the activation energy, R is the gas constant and T is the temperature. [7]

Equation 1

$$r_x = k_x \cdot c_i \cdot \theta_j$$

Equation 2

$$k_x = A_x \cdot e^{\frac{-E_a}{RT}}$$

Reaction rate constants for reactions (8,10-14) are expressed in terms of Arrhenius constant and for the adsorption steps (6,7,9) the collision theory is applied. The difference is found in the expression of the pre-exponential factor. Collision theory is basically based on how probable it is that a specie will stick to the surface when it collides with it. Equation 3 is based on this theory and shows us the surface site density C_s , inner converter surface per volume of area of one mole of active surface site atoms $S_{C,Fe}$, the sticking probability coefficient of specie i $\alpha_{prob,i}$ and total surface coverage Θ . The pre-exponential factor is finally expressed in the equation below (Equation 3). [7] It is assumed that the activation energy for adsorption in general is 0 which makes the reaction rate constant equal to the pre-exponential factor. [8]

Equation 3

$$A_{ads,i} = C'_s S_{C,Fe} \alpha_{prob,i} (1-\theta) \cdot \sqrt{\frac{R \cdot T}{2 \cdot \pi \cdot M_i}} [4, 20]$$

If a closer look is made on the reactions that occur on the Fe sites it can be noticed that the steps included in oxidation of NO are irreversible. For temperatures above 350°C a thermodynamical equilibrium occurs [7]. This means that also the backward reaction is of importance. To get a thermodynamically correct model it is necessary to take into account both the forward and backward reactions. It is also worth to know that the enthalpy- and

entropy change for the gas phase reaction $\text{NO}(\text{g}) + \frac{1}{2} \text{O}_2(\text{g}) \rightarrow \text{NO}_2(\text{g})$ at 600K is -58 kJ/mol and -76 J/(mol*K) respectively and must always be fulfilled. [7] The use of Arrhenius equation (Equation 2) and equation for Gibbs's Free Energy

Equation 6), ΔG makes it possible to implement the calculation of unknown activation energy (E_a) and pre-exponential factor (A). The theory will come to use in the model setup.

Equation 4

$$\Delta G = \Delta H - T \cdot \Delta S = -R \cdot T \cdot \ln K$$

Equation 5

$$K = \frac{k_f}{k_b} = \frac{A_f}{A_b} \cdot \exp\left(-\frac{(E_f - E_b)}{R \cdot T}\right)$$

2.2.2 Parameterisation for Fe-zeolite SCR catalyst

The available starting material in this study included the existing model based on the normal SCR reactions, combined with a program for optimization and experimental data. A set of data values collected from a laboratory scale test were produced by Paul Scherrer Institut (PSI) in Switzerland and experimental data from engine bench test experiments were available from Johnson Matthey (JM) in Sweden.

An existing program called CZM 3.0 which is used for modeling of SCR over Vanadia catalyst was to be used as a template for creating a corresponding program for modeling of SCR over Fe-zeolite catalyst called CZM 4.0. CZM is an abbreviation for cells and zones model and the advantage of this model is its ability to calculate the distribution of species on the catalyst surface and 3D-modeling. Included in the program there was a draft of an optimization program to fit the unknown parameters called parameter optimization tool (POT). This program also needed to be adjusted to function in a satisfying manner.

The reactions included in these two processes, SCR over Vanadia and SCR over Fe-zeolite are very similar which gave the assumption that with only a few changes the task of creating a working program for Fe-zeolite could be accomplished. All chemical reactions and corresponding changes in concentration were modeled in a SimuLink schedule. The existing model was based on three tank reactors in a series to get a balance between the accuracy and computational time. To update the POT and put it into operation, changes to this existing SimuLink model were necessary. The program was set to optimize with *fminsearch*.

2.2.3 Experimental data

Experimental data was obtained from Johnson Matthey and from Paul Scherrer Institut and they were based on both dynamical and steady state experiments. The data from Johnson Matthey was performed in an engine cell using a full scale catalyst whereas the experiments from PSI were lab scale experiments. The dimensions of the Fe-ZSM5 catalyst from Johnson Matthey and Paul Scherrer Institut respectively are listed in the Table 1:

Fe-ZSM5	PSI	JM
Volume catalyst 1	8.05 cm ³	19288.05 cm ³
Volume catalyst 2	15.02 cm ³	-
Volume catalyst 3	16.54 cm ³	-

Table 1. Dimensions of Fe-ZSM5 catalyst

The data set from Johnson Matthey was produced two dynamical experiments regarding the temperature and one steady state experiment varying the following parameters:

- Mass flow of exhaust gases (kg/s)
- Temperature before and after catalyst (°C)
- Concentration of NO, NO₂ and NH₃ before and after the catalyst (ppm-mol)

The measurement time for each dynamical experiment was approximately 90 minutes and the temperature was varied in a range between ca 200-450°C after the catalyst. This data set is supposed to be used in validation purpose.

Paul Scherrer Institut produced fifteen dynamical experiments with respect to the inlet flows of NO_x and NH₃. There were also twenty five steady state experiments available. In most of the experiments the NO_x feed was kept constant at 500 ppm with intervals of 25, 50, 75 and 100 % of NO respectively. The steady state experiments were based on three different Gas Hourly Space Velocities (GHSV h⁻¹)¹ and a temperature range between 200-500°C for each GHSV 21700 h⁻¹, 28800 h⁻¹ and 52000 h⁻¹. For each temperature and GHSV the NH₃ oxidation was measured by switching NH₃ on and off at 0.8*αOD², 1*αOD and 1.2*αOD. During the NH₃ steps equilibration was awaited and thus steady-state points were available. From each steady state experiment it was possible to extract between four to sixteen steady state values depending on the experiment. An extraction of values from all steady state data sets and a combination of these gave a set of totally 280 points. Variables included in the dynamical data sets from Paul Scherrer Institut were the same as those from Johnson Matthey but the dynamical experiments from Paul Scherrer Institut was isothermal. The amount of data points in each dynamical experiment was approximately between 5000-7000. The dynamic behaviour was also tested at 0.8*αOD, 1*αOD and 1.2*αOD but with 30, 60, 120 and 240 second NH₃ pulses separated by pauses of the same length. Some experiments will be used for optimization and the other sets for validation.

2.2.4 Model setup

The model for the Fe-zeolite is based on three tank reactors in a series as mentioned earlier. The input and output variables for each tank are shown in Figure 13. The biggest changes from the previous vanadia-based SCR model were made in the modelling of reactions that occur on the iron sites. All adsorption steps were modelled according to the

¹ Gas Hourly Space Velocity (GHSV): Commonly used in industry

² αOD means the optimum dosage ratio of NH₃/NO_x in the feed under practice-relevant conditions that results in a slip of 10 ppm ammonia

downstream of the catalyst. 23.Manfred Koebel, M.E.a.G.M., *Recent Advances in the Development of Urea-SCR for Automotive Applications*. SAE 0148-7191, 2001: p. 12.

collision theory. In the model it is assumed that the NO oxidation occurs at the iron sites and all other reactions occur on the zeolite sites.

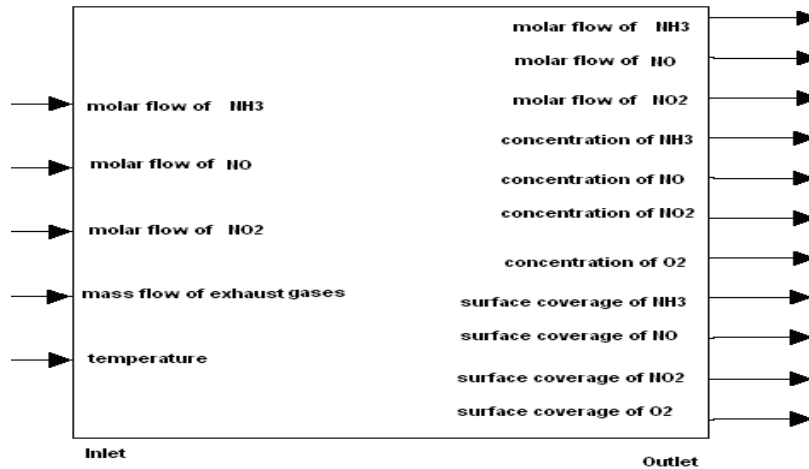


Figure 13 Input and output variables a tank

2.2.5 Iron sites

We also decided to model this reaction pathway according to this mechanism but with more detail. In the model shown in Figure 14 it was assumed that both oxygen and nitrogen oxide adsorb and then a surface reaction occurs where NO₂ is produced. For the same model it is further assumed that all species that adsorb also desorb and that the oxidation reaction is reversible.

Langmuir-Hinshelwood

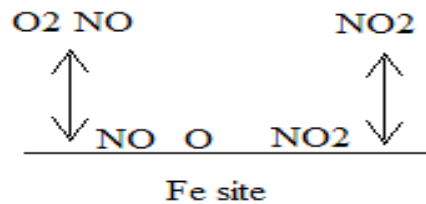


Figure 14 Reaction that occur on iron site

Figure 15 shows the energy diagram that was used to express pre-exponential factor and the activation energy for reduction of NO₂ in combination with

Equation 6 and

Equation 7. Activation energies of the adsorption steps are set to zero which makes this expression possible.

Equation 6

$$\Delta G = \Delta H - T \cdot \Delta S = -R \cdot T \cdot \ln K$$

Equation 7

$$K = \frac{k_f}{k_b} = \frac{A_f}{A_b} \cdot \exp\left(-\frac{(E_f - E_b)}{R \cdot T}\right)$$

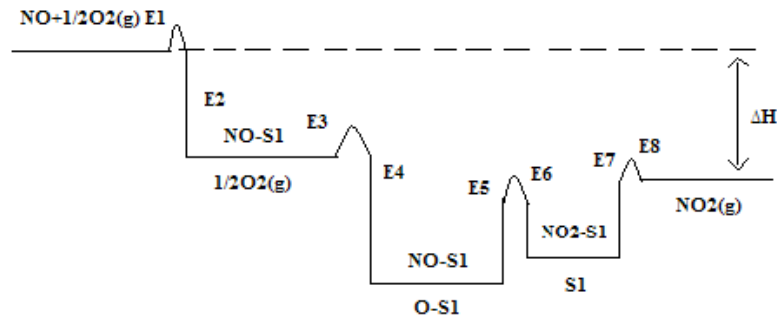
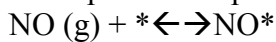


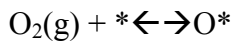
Figure 15 Energy diagram Langmuir-Hinshelwood: adsorption/desorption of NO, adsorption/desorption of O₂, oxidation of NO and reduction of NO₂, desorption/adsorption/ of NO₂ [8]

Adsorption/desorption of Nitrogen oxide:


Equation 8

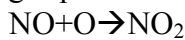
$$r_{ads/des,NO} = C'_S S_{C,Fe} \alpha_{prob,NO} \theta \cdot c_{NO} \sqrt{\frac{R \cdot T}{2 \cdot \pi \cdot M_{NO}}} - C_S^{Fe} k_{des,NO} \cdot e^{-\frac{E_{des,NO}}{RT}} \theta_{NO}$$

Dissociative adsorption of oxygen, gas phase oxygen excess:


Equation 9

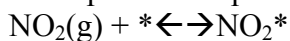
$$r_{ads/des,O_2} = C'_S S_{C,Fe} \alpha_{prob,O_2} \theta \cdot c_{O_2} \sqrt{\frac{R \cdot T}{2 \cdot \pi \cdot M_{O_2}}} - C_S^{Fe} k_{des,O_2} \cdot e^{-\frac{E_{des,O_2}}{RT}} \theta_O$$

Formation of NO₂ on the Fe sites, and immediate desorption of Nitrogen dioxide into the gas phase:


Equation 10

$$r_{NO_{ox}/NO_{2,red}} = k_{ox,NO} \theta_{NO} \theta_O e^{-\frac{E_{red,NO}}{RT}} - k_{red} \theta_{NO_2} \cdot c_{NO_2} \cdot e^{-\frac{E_{red,NO_2}}{RT}}$$

Adsorption/desorption of Nitrogen dioxide:


Equation 11

$$r_{ads/des,NO_2} = C'_S S_{C,Fe} \alpha_{prob,NO_2} \theta \cdot c_{NO_2} \sqrt{\frac{R \cdot T}{2 \cdot \pi \cdot M_{NO_2}}} - C_S^{Fe} k_{des,NO_2} \cdot e^{-\frac{E_{des,NO_2}}{RT}} \theta_{NO_2}$$

2.2.6 Zeolite-sites

All reactions on the Fe sites are assumed to occur by an Eley-Rideal mechanism. The ammonia is adsorbed, the other species do a “fly by pick up” and the reactions occur as shown in Figure 16:

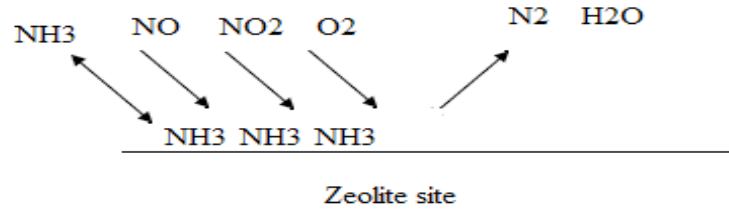


Figure 16. Reaction that occur on zeolite site [9]

Ammonia Adsorption:
 $\text{NH}_3 + \text{S} \rightarrow \text{NH}_3(\text{S})$

Equation 12

$$r_{ads,NH_3} = C_S S_C \alpha_{prob} (1 - \theta_{NH_3}) \cdot c_{NH_3} \sqrt{\frac{R \cdot T}{2 \cdot \pi \cdot M_{NH_3}}}$$

Ammonia Desorption:
 $\text{NH}_3(\text{S}) \rightarrow \text{NH}_3 + \text{S}$

Equation 13

$$r_{des,NH_3} = C_S k_{des,NH_3} \theta_{NH_3} e^{-\frac{E_{des}}{RT}}$$

Standard SCR:
 $4\text{NH}_3 + 4\text{NO} + \text{O}_2 \rightarrow 4\text{N}_2 + 6\text{H}_2\text{O}$

Equation 14

$$r_{NO} = C_S \theta_{NH_3} c_{NO} k_{NO} \cdot e^{-\frac{E_{NO}}{RT}}$$

Fast SCR:
 $4\text{NH}_3 + 2\text{NO} + 2\text{NO}_2 \rightarrow 4\text{N}_2 + 6\text{H}_2\text{O}$

Equation 15

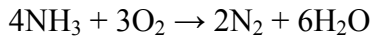
$$r_{NO,NO_2} = C_S \theta_{NH_3} c_{NO}^{1/2} c_{NO_2}^{1/2} k_{NO,NO_2} \cdot e^{-\frac{E_{NO,NO_2}}{RT}}$$

Slow SCR:
 $8\text{NH}_3 + 6\text{NO}_2 \rightarrow 7\text{N}_2 + 12\text{H}_2\text{O}$

Equation 16

$$r_{NO_2} = C_S \theta_{NH_3} c_{NO_2}^{3/4} k_{NO_2} \cdot e^{-\frac{E_{NO_2}}{RT}}$$

Ammonia oxidation:



Equation 17

$$r_{\text{O}_2} = C_s \theta_{\text{NH}_3} k_{\text{O}_2} \cdot e^{-\frac{E_{\text{O}_2}}{RT}}$$

Concentration variations

The concentration in each tank reactor is set to be constant. The variation of concentration over time for tank i is presented below.

$$\frac{dc_i}{dt} = \frac{-R_{s,EG} \cdot m_{EG}^* \cdot T_{EG}}{\varepsilon \cdot A_{fr} \cdot P_{amb} \cdot M_{air}} \cdot \frac{(c^{i-1} - c^i)}{L/N}$$

The variation of the gas phase concentration of ammonia over time:

Equation 18

$$\frac{dc_{\text{NH}_3}}{dt} = \frac{-R_{s,EG} \cdot m_{EG}^* \cdot T_{EG}}{\varepsilon \cdot A_{fr} \cdot M_{air} \cdot P_{amb}} \cdot \frac{d}{dx}(c_{\text{NH}_3}) + r_{des} - r_{ads}$$

The variation of the gas phase concentration of NO over time:

Equation 19

$$\frac{dc_{\text{NO}}}{dt} = \frac{-R_{s,EG} \cdot m_{EG}^* \cdot T_{EG}}{\varepsilon \cdot A_{fr} \cdot M_{air} \cdot P_{amb}} \cdot \frac{d}{dx}(c_{\text{NO}}) - r_{\text{NO}} - r_{\text{NO},\text{NO}_2} - r_{ads,\text{NO}}$$

The variation of the gas phase concentration of NO2 over time:

Equation 20

$$\frac{dc_{\text{NO}_2}}{dt} = \frac{-R_{s,EG} \cdot m_{EG}^* \cdot T_{EG}}{\varepsilon \cdot A_{fr} \cdot M_{air} \cdot P_{amb}} \cdot \frac{d}{dx}(c_{\text{NO}_2}) - r_{\text{NO}_2} - r_{\text{NO},\text{NO}_2} + r_{\text{NO}_2,\text{Fe}}$$

The variation of the coverage of ammonia on the zeolite sites over time:

Equation 21

$$C_s \frac{d\theta_{\text{NH}_3}}{dt} = r_{ads} - r_{des} - r_{\text{NO}} - r_{\text{NO}_2} - r_{\text{NO},\text{NO}_2} - r_{\text{O}_2}$$

The variation of the coverage of NO on the Fe sites over time:

Equation 22

$$C_s^{Fe} \frac{d\theta_{\text{NO}}}{dt} = r_{ads/des,\text{NO}} - r_{\text{NO}_{ox}/\text{NO}_2,\text{red}}$$

The variation of the coverage of NO2 on the Fe sites over time:

Equation 23

$$C_S^{Fe} \frac{d\theta_{NO_2}}{dt} = r_{NO_{ox}/NO_{2,red}} + r_{ads/des,NO_2}$$

The variation of the coverage of O on the Fe sites over time:

Equation 24

$$C_S^{Fe} \frac{d\theta_O}{dt} = r_{ads/des,O} - r_{NO_{ox}/NO_{2,red}}$$

The POT tool also included a program for optimization of a thermal model. The thermal model describes the difference between the heat added from the exhaust gas flow and the radiation losses. The heat released by the reactions is assumed to be negligible compared to the thermal energy transferred by convection. Therefore the temperature modelling is remained the same as in the draft. [9]

The variation of temperature over time for tank i is presented below:

Equation 25

$$\frac{dT_i}{dt} = \frac{n_{cell} \cdot c_{p,EG} \cdot m_{EG}^*}{c_{p,c} \cdot m_c} \cdot (T_{i-1} - T_i) - \frac{\epsilon_{rad,SCR} \cdot \sigma_{SB} \cdot A_{rad,SCR}}{c_{p,c} \cdot m_c} \cdot (T_i^4 - T_{amb}^4)$$

2.2.7 Parameterization

The first step in the optimization process was to parameterize the efficiency factor/radiation ($\epsilon_{rad,SCR}$) and the heat capacity ($C_{p,c}$) of the thermal model. The optimization was made on basis of four different experimental sets of data. Two data sets each from PSI and JM respectively were available. One data set each from PSI and JM were used for optimization which was carried out with both `fminsearch` and `lsqnonlin`. The other files were left for validation.

The next step in the optimization process was to choose the starting values of the parameters in the kinetic model. It is of great importance to choose the parameter values which provide the same magnitude of the modeled values as the experimental values have, to tune in an approximate fitting. [10] It was also necessary to change some operating settings in the ODE solver and `lsqnonlin`. The changes made:

- Ode15s: Default: RelTol = 10^{-3} , AbsTol = 10^{-6}
Change: RelTol = 10^{-7} , AbsTol = 10^{-7}
- Lsqnonlin: Default: TolFun = 10^{-6} , TolX = 10^{-6} , step length = 10^{-8}
Change: TolFun = 10^{-12} , TolX = 10^{-12} , step length = 10^{-2}

The choice of starting values for some of the parameters was partially based on contact with Professor Enrico Tronconi of the Politecnico di Milano. He suggested that the values which were included in the article by Chatterjee et al, 2007 were good start values for our model. There were also wild guesses made for some unknown parameters of the collision theory which could not be found in any literature. The proposed values were used in the model, and were showed to produce model values of the same magnitude as the

experimental data values after tuning in the guessed parameters. These values from the aforementioned article were based on a model for SCR over Fe-zeolite. Starting values for desorption of NO₂ and O₂ were taken from Olsson et.al. [7] and are for a SCR model over Cu-zeolite. All selected literature values are listed in the Table 2.

Reactions	Activation energy (J/mol)	Pre-exponential	Reference
Desorption of NO	114000	$5.3 \cdot 10^{10}$ mol/s kg-cat	[11]
Desorption of NH ₃	92048	$2.597 \cdot 10^9$ m ³ /mol s	[12]
Desorption of NO ₂	141500	$3.2 \cdot 10^{12}$ mol/(s kg-cat)	[11]
Desorption of O ₂	48800	$3.2 \cdot 10^{12}$ mol/(s kg-cat)	[11]
Standard SCR	48701.76	$3.236 \cdot 10^{10}$ m ³ /mol s	[12]
Fast SCR	51305.168	$5.331 \cdot 10^8$ m ³ /mol s	[12]
Oxidation of NO	31066.056	$6.478 \cdot 10^3$ m ³ /mol s	[12]
Oxidation of NH ₃	175728	$3.135 \cdot 10^{13}$ m ³ /mol s	[12]

Table 2. Selected literature values

Totally there are twenty six parameters in the model. Thirteen of these were not found in literature that apply to a kinetic model for Fe-zeolite catalysts and were thus initially set to vary. In the beginning a tuning of these unknown parameters was necessary so that the model values come in the same magnitude range as the experimental values. For this purpose the *random method* described earlier was used. After the tuning six of the unknown parameters (α_{probNH_3} α_{probNO} α_{probO_2} α_{probNO_2} k_{NO_2} E_{NO_2}) were fixed. Then a run with twenty parameters was started. This was done with the *lsqnonlin* solver which we assumed would have a better chance of finding a minimum and thus improving the parameter values.

The experimental data used was the collection of the steady state points and four dynamical data sets with different Gas Hourly Space Velocities and temperatures. The thought behind the choice of experiments was to optimize the model for different conditions. The files listed below were chosen because they were functional with the different default settings in MatLab/Simulink.³

- GHSV 21700 for temperature 200°C
- GHSV 28800 for temperatures 200°C, 250°C and 300°C

In the end a validation was made to see how successful the parameterization was. The dynamical data sets on which the validation was made are:

- GHSV 52000 for temperature 200°C
- GHSV 52000 for temperature 400°C

³ The range of experiments that were to be used originally for the optimization is listed bellow. They were not used because they were not functional with the default MatLab/Simulink settings.

- ☐ GHSV 21700 for temperature 200°C
- ☐ GHSV 21700 for temperature 400°C
- ☐ GHSV 28000 for temperature 350°C
- ☐ GHSV 52000 for temperature 200°C
- ☐ GHSV 52000 for temperature 400°C

2.2.8 Results

2.2.8.1 Thermal Model

The thermal model optimization was successful with both `fminsearch` and `lsqnonlin`. The different tools gave the same result which follow below.

Figure 14 from Appendix A shows the modelled values after optimization with one of the dynamical experiments from JM. It can be seen that the modelled values for outlet temperature match the measured values for outlet temperature perfectly. There were no complications in optimizing the model for the data set from PSI. Almost the same great compliance between measured and simulated values was achieved in that case as well. Despite the successful optimization the parameter values optimized with experimental values from PSI were considered incorrect due to the few measured points in the set. Figure 15 in Appendix A shows the optimized model validated with the other data set from JM and it can be seen that the model matches the validation data.

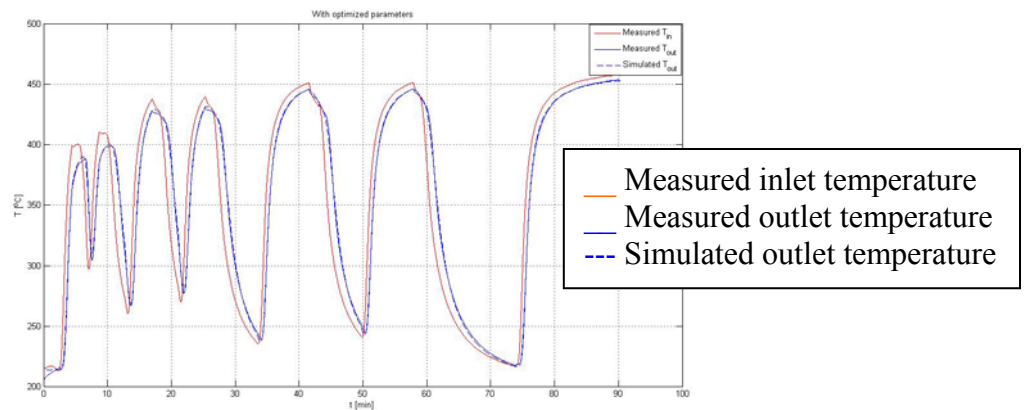


Figure 17 Model against data set for optimization. The measured values of inlet and outlet temperature and the simulated outlet temperature plotted against time.

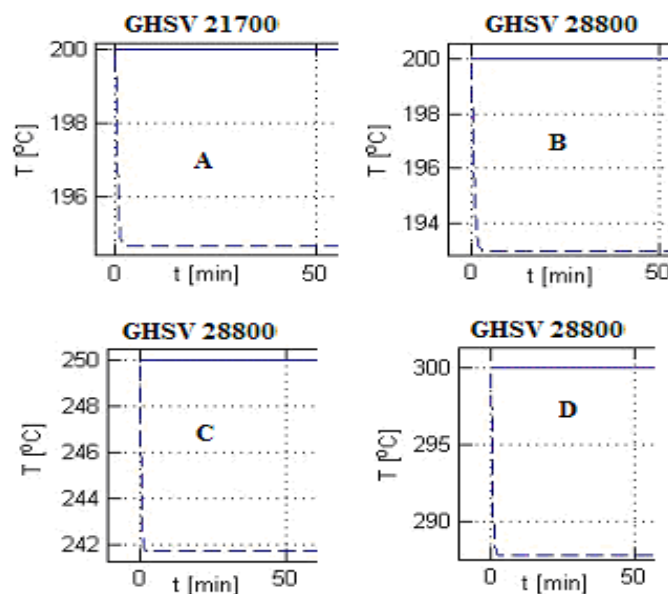


Figure 18 The figure shows the difference in temperature over time between measured and simulated data for two different GHSV.

2.2.8.2 Kinetic model

The optimization of parameters with random method and lsqnonlin gave following results. The difference in temperature over time between measured temperatures and the simulated temperatures produced by the thermal model are shown in Figure 18 for the four different dynamical data sets used in the optimization of the kinetic model. It can be seen that the existing difference in temperature between measured and simulated values will increase with increased temperature or/and GHSV.

The injection of NO, NO₂ and NH₃ over time is presented in Figure 19 for the four different dynamical data sets. The following figures (Figure 20 Figure 21 Figure 22) in Appendix A are showing the simulated model and measured outlet values. The last figure (Figure 23) presents the validation of dynamical data points for optimized parameters. There is even some close ups presented for two different data sets which shows how close the simulated data with optimized parameters is to the measured data. Figure 23

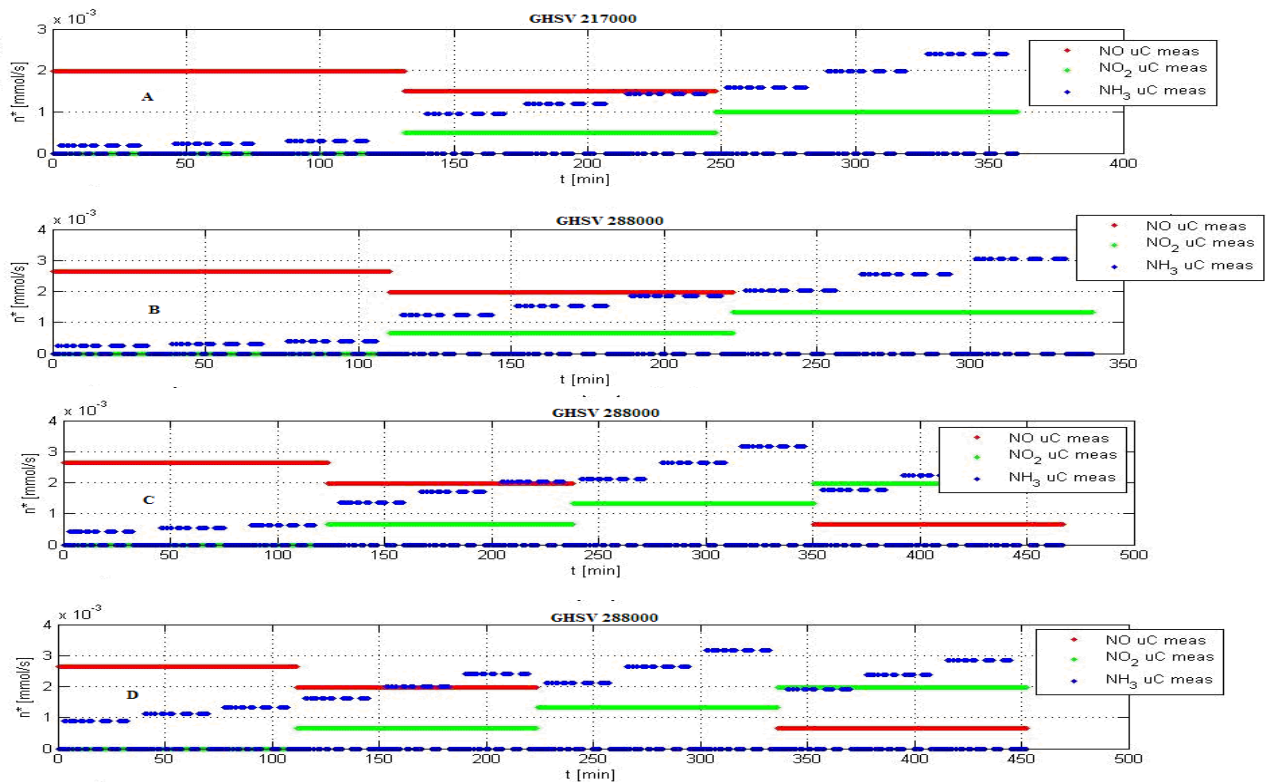


Figure 19 The figure shows the injection of NO, NO₂ and NH₃ over time.

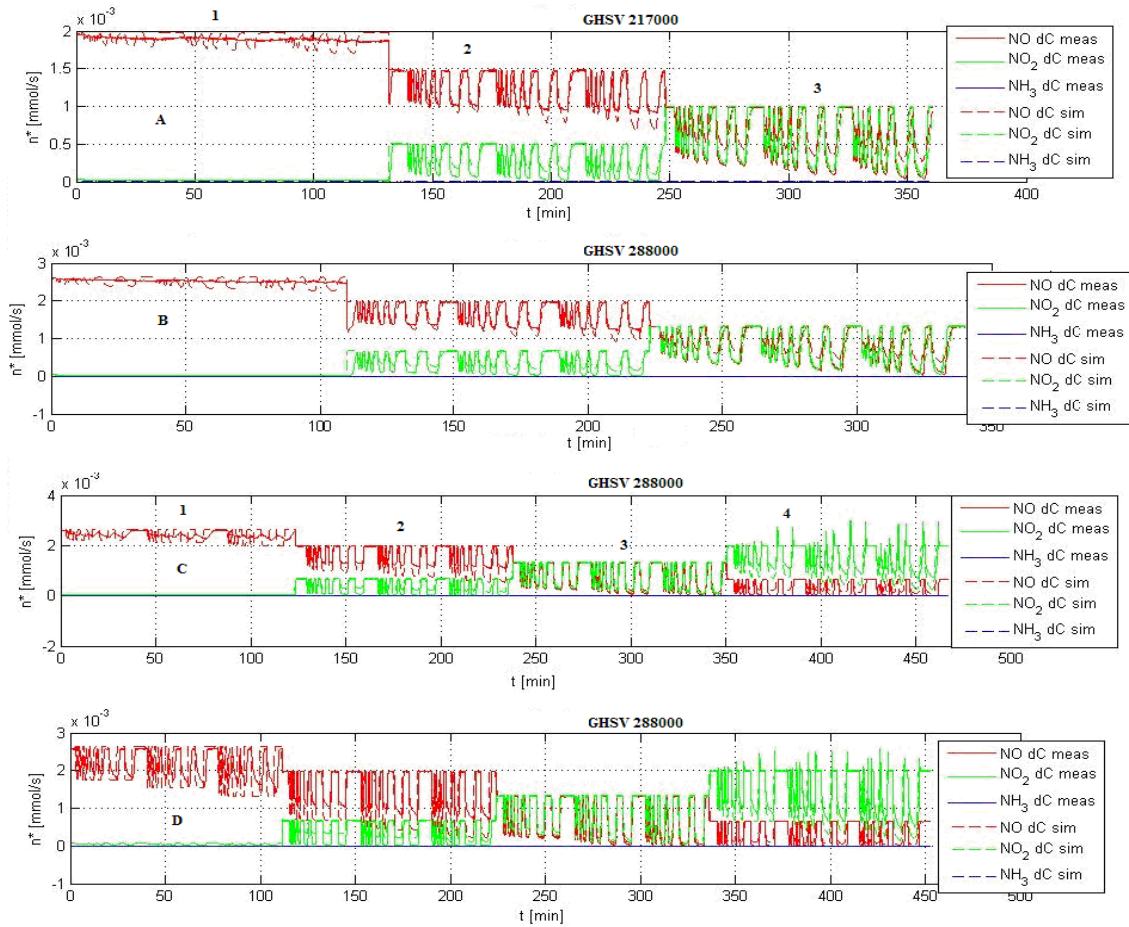


Figure 20 The figure shows simulated model and measured outlet values.

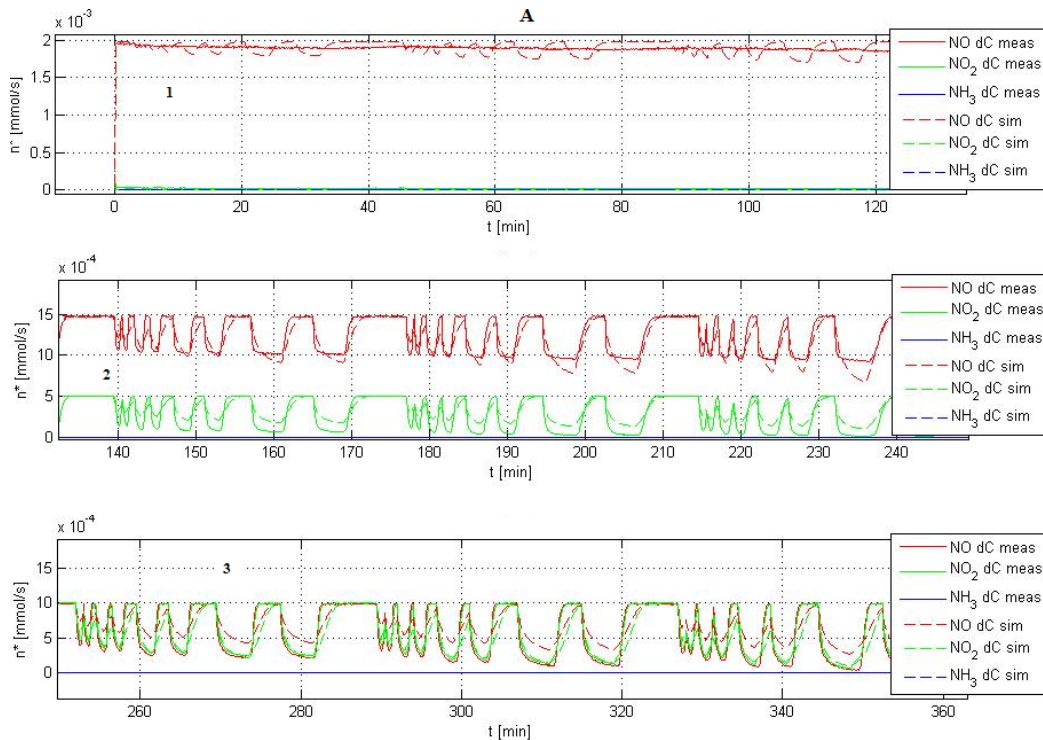


Figure 21 The figure shows close up segments of simulated model and measured outlet values.

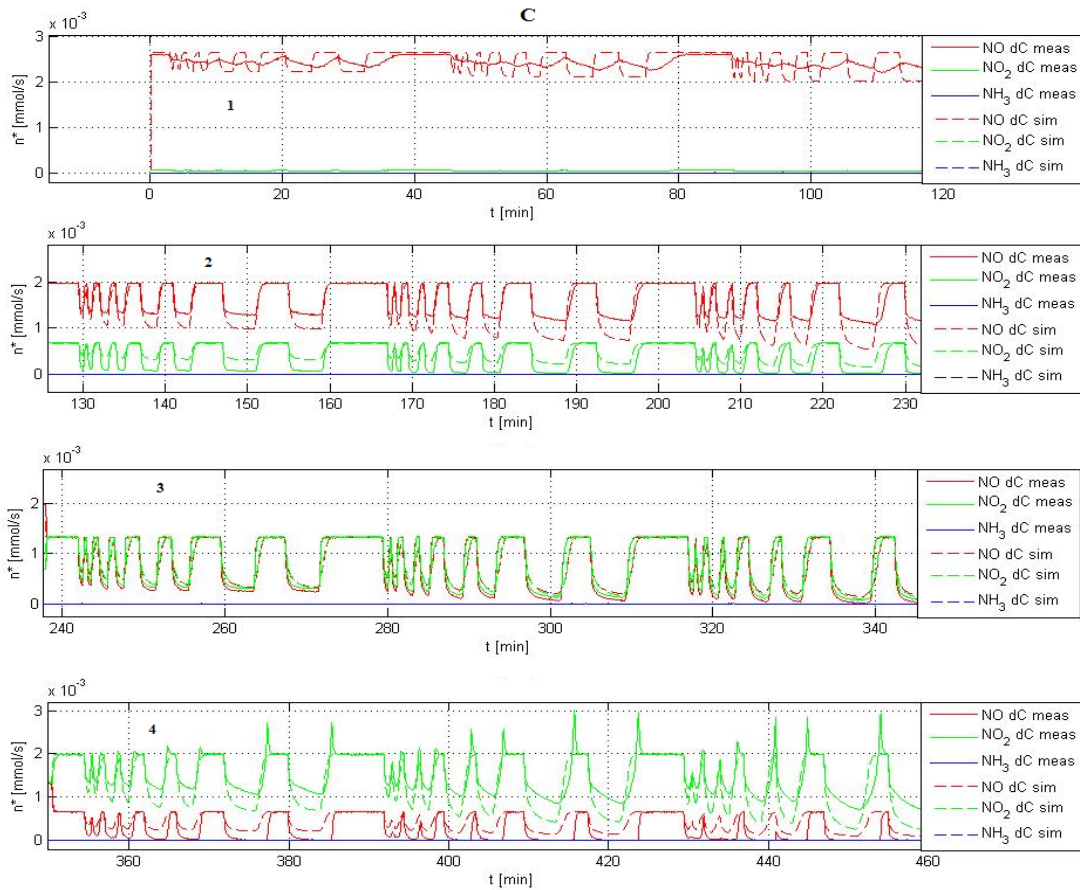


Figure 22. The figure shows close up segments of simulated model and measured outlet values.

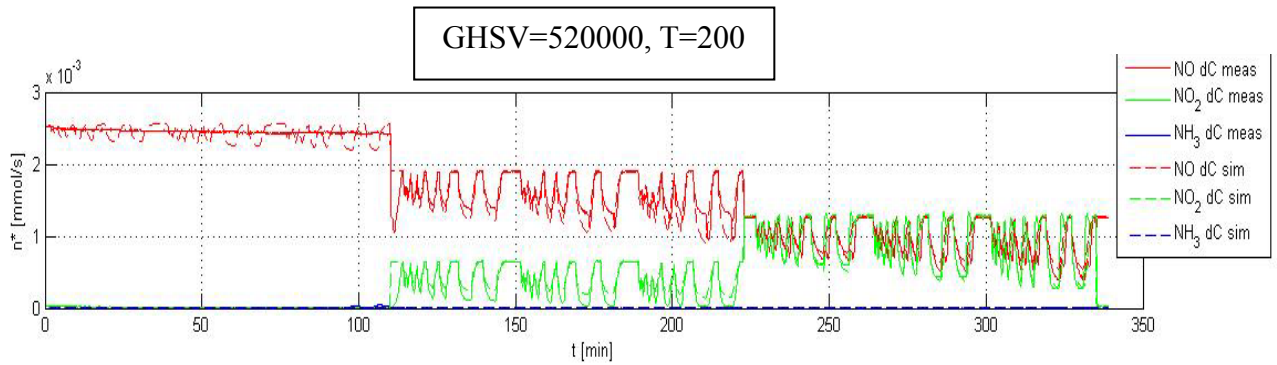


Figure 23. The figure shows simulated model and measured outlet values used for validation.

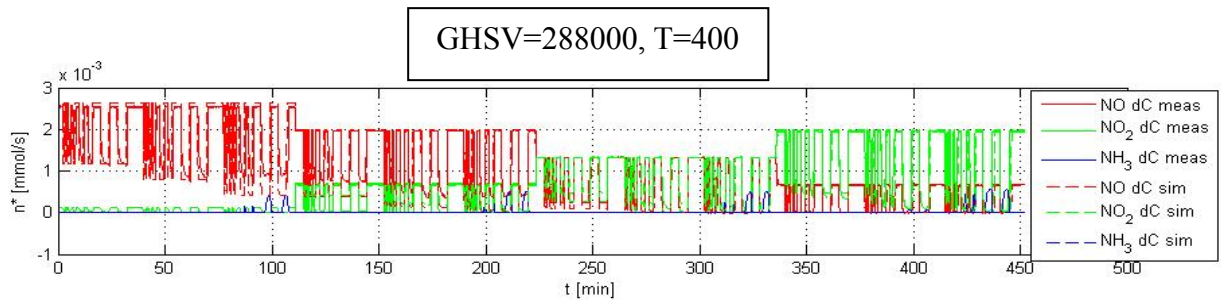


Figure 24. The figure shows simulated model and measured outlet values used for validation.

2.2.9 Discussion

The validation carried out indicates that both the kinetic and thermal models with the optimized parameters show good agreement with experimental validation data. The comparison shows that the simulated lines for all subjects follow the measured data points.

The thermal parameter values produced in the optimization process were compared with values available on Swenox AB. It showed that the calculated parameter values were in the same magnitude as the validation values. These values can thus be relevant in further work. The results in Figure 18 are found to be incorrect. Looking at equation 21 one can see that according to the model setup, the temperature difference between the measured and simulated values should decrease with increasing gas flow and increase with increasing temperature. Explanation for the misleading results can be located to the way the experiments were performed. In this case the catalysts were constantly heated during the experiments. This means that for the experiments there were no heat losses due to radiation and thus the model with the radiation losses does not apply. The optimized model should be validated with other more relevant experimental data values.

From the resulting parameter values it can be noticed that the sticking probability for NO_2 is close to one which means that almost all nitrogen dioxide molecules adsorb on the iron surface on collision. In the same way the model predicts that it is very unlikely that a NO molecule will stick to the iron surface on collision due to a small sticking probability. Further it can be concluded that most of the final parameter values are in the same magnitude as the starting parameter values. This indicates that the model is sensitive to small changes in parameter values.

As we mentioned the validation of the optimized kinetic model showed a good agreement with experimental data. Although the model has good overall match there are some noticeable differences. For example the first region in Figure 19 and Figure 20 it can be seen that for small amounts of ammonia in the feed and at low temperatures the model is not following the measured values. An explanation of this can be that ammonia is stored and does not react under these conditions. For the case with higher temperature and higher amount of ammonia (Figure 22) it can be seen that the model is valid. Under these conditions ammonia reacts immediately. In Figure 22 at the end of every region there are ammonia "peaks". This could indicate that there is ammonia slip due to over dosage. The model does not predict the ammonia slip correctly due to lack of ammonia slip in experimental values used for the optimization. Other differences that exist can be explained by differences in the number of data points in the steady state data set compared with the amount of points in the dynamical data sets. This means that the steady state points are relatively few and can in this case be seen as a disturbance in the optimization process. To get around this problem the experiments could be weighted and thus be equally valued.

There are still things that can be done to improve the performance of the optimization process as well as the fitting. One thing that can be made in the further work is to analyse the jacobian matrix and the residuals in Simca. Simca is a program for multivariate statistical analysis which can facilitate the choice of significant parameters in a certain

model by analyzing the jacobian matrix and residuals.[13] Such an analysis can give how different parameters affect the model values and how much. Even the relationship between parameters can be analysed. This can be used to decrease amount of parameters that vary which decreases the optimization time. With the jacobian it is possible to calculate a so called condition number. A low condition number (10^4) means that all parameters play an important roll and for high condition number (10^{12}) indicates that some parameters are less important then others and can be fixed. For the optimized model in this project the condition number was in the magnitude of 10^4 .

In this project the parameters step length was set to be the same for all parameters. It can be helpful to know that this step length can be specified for each parameter. If the optimal step length for each parameter is found, the result can contribute to better fitting.

2.2.10 Conclusion

The parameter optimization tool for Fe-exchanged zeolite catalysts in combination with the model presented in this work can now be used to fit the parameter values to experimental steady state data set combined with several dynamical data sets. With the given settings, and taking into account the number of parameters the optimization process takes about 12 hours which can be considered as relatively fast. According to the results the parameters optimised by the described parameterisation can be used in simulation purpose for low temperatures.

2.2.11 Symbols

GHSV	Gas Hourly Space Velocities
*	Adsorbed onto the catalyst surface
α_{probNH_3}	Sticking probability of NH_3 on zeolite sites at zero coverage
α_{probNO}	Sticking probability of NO on Fe sites at zero coverage
α_{probO_2}	Sticking probability of O_2 on Fe sites at zero coverage
α_{probNO_2}	Sticking probability of NO_2 on Fe sites at zero coverage
$A_{\text{rad,SCR}}$	Surface area of catalyst
$C_{\text{p,c}}$	Specific heat of the catalyst at constant pressure
$C_{\text{p,EG}}$	Specific heat of the exhaust gas at constant pressure
$C_{\text{S,Fe}}$	Surface site density of Fe sites (concentration of active surface atoms with respect to gas volume in converter)
C_{S}	Surface site density of zeolite sites (concentration of active surface atoms with respect to gas volume in converter)
c_{NH_3}	Gas phase concentration of NH_3
c_{NO}	Gas phase concentration of NO
c_{NO_2}	Gas phase concentration of NO_2
c_{O_2}	Gas phase concentration of O_2
$\epsilon_{\text{rad,SCR}}$	Efficiency factor or radiation
E_{red}	Activation energy for reduction of NO_2
$E_{\text{des,NO}}$	Activation energy for desorption of NO
$E_{\text{des,O}_2}$	Activation energy for desorption of O_2
$E_{\text{des,NO}_2}$	Activation energy for desorption of NO_2
E_{des}	Activation energy for NH_3 desorption from zeolite sites
E_{NO}	Activation energy the standard SCR
E_{NO_2}	Activation energy for reduction of NO_2 with NH_3
$E_{\text{NO,NO}_2}$	Activation energy the fast SCR
$E_{\text{ox,NO}}$	Activation energy for oxidation of NO
E_{O_2}	Activation energy for oxidation of NH_3
k_{red}	Pre-exponential for reduction of NO_2
k_{des}	Pre-exponential for desorption of NH_3 from zeolite sites
k_{NO}	Pre-exponential for the standard SCR
k_{NO_2}	Pre-exponential for reduction of NO_2 with NH_3
$k_{\text{NO,NO}_2}$	Pre-exponential for the fast SCR
k_{O_2}	Pre-exponential for oxidation of NH_3
$k_{\text{des,NO}}$	Pre-exponential for desorption of NO
$k_{\text{des,O}_2}$	Pre-exponential for desorption of O_2
$k_{\text{des,NO}_2}$	Pre-exponential for desorption of NO_2

$k_{\text{ox,NO}}$	Pre-exponential for oxidation of NO
M_{NH_3}	Molar mass of NH_3
M_{NO}	Molar mass of NO
M_{O_2}	Molar mass of O_2
M_{NO_2}	Molar mass of NO_2
M_{air}	Molar mass of air
m_c	Mass of catalyst
m	Exhaust gas mass flow
n_{cell}	Number of cells along the catalyst used in the model
R	Universal gas constant
r_{ads}	Rate of adsorption of NH_3
r_{des}	Rate of desorption of NH_3
r_{NO}	Rate of standard SCR reaction
r_{NO_2}	Rate of reduction of NO_2 with NH_3
$r_{\text{NO,NO}_2}$	Rate of the fast SCR reaction
r_{O_2}	Rate of oxidation of NH_3
$r_{\text{ads/des}}$	Rate of adsorption of NO on Fe type sites
$r_{\text{NO,ox/NO}_2,\text{red}}$	Rate of formation of NO_2 on Fe type sites
$r_{\text{ads,O}_2}$	Rate of dissociative adsorption of O_2 on Fe type sites
σ_{SB}	Radiation constant
$S_{\text{C}_{\text{NH}_3}}$	Inner converter surface per volume or area of one mole of active zeolite surface site atoms
$S_{\text{C}_{\text{Fe}}}$	Inner converter surface per volume or area of one mole of active Fe surface site atoms
Θ	Free coverage
$\Theta^{\text{Fesite}}_{\text{tot}}$	Total coverage of the Fe sites
Θ_{NH_3}	Coverage of NH_3 on zeolite type sites
Θ_{NO}	Coverage of NO on Fe type sites
Θ_{O}	Coverage of oxygen atoms on Fe type sites
Θ_{NO_2}	Coverage of NO_2 on the Fe type sites
T	Temperature

2.2.12 Symbol units

GHSV	$[\text{h}^{-1}]$
α_{prob}	$[-]$
$A_{\text{rad,SCR}}$	$[\text{m}^2]$
C_p	$[\text{J}/(\text{K}\cdot\text{kg})]$
C_s	$[\text{mol}/\text{m}^3]$
c	$[\text{mol}/\text{m}^3]$ or $[\text{ppm}]$
ε	$[-]$
E	$[\text{J}/\text{mol}]$
k	Depending on reaction
M	$[\text{kg}/\text{mol}]$
m_{EG}^*	$[\text{kg}/\text{s}]$
R	$[\text{J}/(\text{K}\cdot\text{mol})]$
r	$[\text{mol}/(\text{s}\cdot\text{m}^3)]$
σ_{SB}	$5.67\cdot 10^{-8} [\text{W}/(\text{m}^2\cdot\text{K}^4)]$

Sc	[m ² /m ³] or [mol/m ³]
Θ	[-]
T	[K]

2.2.13 Chemical species

Fe	Iron
H ₂ O	Water
N ₂	Nitrogen gas
NH ₃	Ammonia
NO	Nitrogen oxide
NO ₂	Nitrogen dioxide
O	Oxygen atom
O ₂	Oxygen gas

3 Bibliography

1. Åsa Johansson, User Guide Cells and Zones model version 3.0, 2007.
2. Christoph Michael Schär, Cells-&-Zones model User's Guide, 2004.
3. R. Bird et al. Transport Phenomena, Wiley, 1960, ISBN: 047107392
4. R. C. Reid et al, McGraw Hill, Properties of gases and liquids (4th edition), 1987, ISBN. 0070517991.
5. T. Deuschle et al., Numerical Simulation of the Filtration and Regeneration in Diesel Particulate Traps, World filtration congress, 2004, New Orleans.
6. J.C. Wurzenberger, S. Kutsch, Advanced Simulation Technologies for Diesel Particulate Filters, A Modeling Study on Asymmetric Channel Geometries, SAE world congress 2007, 2007-01-1137
7. L. Olsson, *Fundamental Studies of Catalytic NO_x Removal*, in *Department of Chemical Reaction Engineering*. 2002, Chalmers University of Technology: Gothenburg.
8. L. Olsson., Personal Communication (Thermodynamics). 2008: Gothenburg.
9. Å. Johansson, User guide Cells and Zones model: Version 4.0 Zeolite catalyst kinetics. 2008.
10. B. Andersson., Personal Communication 2008: Gothenburg.
11. L. Olsson, H.S., Richard J. Blint, *Detailed Kinetic Modeling of NO_x adsorption and NO oxidation over Cu-ZSM-5*. Applied Catalysis B: Environmental, 2008(2008): p. 48.
12. D. Chatterjee, M. Weibel, I. Nova, A. Grossale, E. Tronconi *Numerical Simulation of Zeolite- and V-Based SCR Catalytic Converters*. SAE 0148-7191, 2007: p. 14.
13. J. Sjöblom, *Personal Communication (Simca)*. 2009: Gothenburg.